ACS OMEGA

Open Access

http://pubs.acs.org/journal/acsodf

Article

Simultaneous Determination of Chemical Oxygen Demand, Total Nitrogen, Ammonia, and Phosphate in Surface Water Based on a Multielectrode System

Xinyue Jiang, Defu Liu,* Guodong Jiang, and Yuqun Xie*

Cite This: *ACS Omega* 2024, 9, 29252−29262

Read Online

ACCESS | Metrics & More | Article Recommendations | Supporting Information

ABSTRACT: A technique for monitoring chemical oxygen demand (COD), total nitrogen (TN), ammonia (N-NH_4), and phosphate (P-PO_4) in surface water with a targeted signal multielectrode system (Cu, Ir, Rh, $Co(OH)_2$, and $Zr(OH)_4$ electrodes) is proposed for the first time. Each water quality index is specifically detected by at least two electrodes with distinct selectivity sensing mechanisms. Cyclic voltammetry and electrochemical impedance measurements are employed for multidimensional signal acquisition, complemented by normalization and Least Absolute Shrinkage and Selection Operator (LASSO) for principal feature extraction and dimension reduction. Multiple linear regression (MLR), partial least-squares (PLS), and eXtreme Gradient Boosting (XGBoost) were employed to evaluate the established prediction model. The precisions of the multielectrode system are ±10%/±5 ppm of COD, ±10%/±0.2 ppm of TN, ±5%/±0.1 ppm of N-NH_4, and ±5%/±0.01 ppm of P-PO_4. The analysis time of the multielectrode system is reduced from hours to minutes compared with traditional analysis, without any sample pretreatment, facilitating continuous online monitoring in the field. The developed multielectrode system offers a feasible strategy for online *in situ* monitoring of surface water quality.

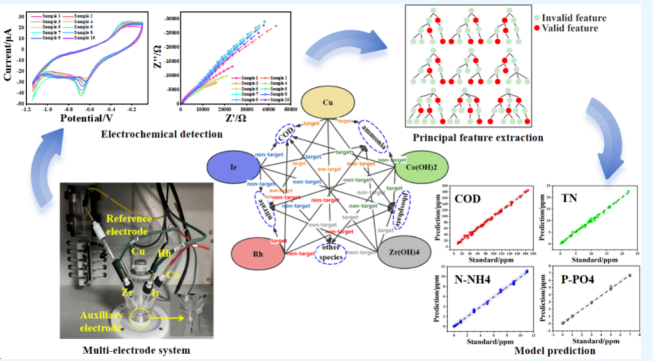

1. INTRODUCTION

Assessing the quality of environmental water and soil is paramount for the health, economy, and sustainability of any region.[1] Pollutants from industrial, agricultural, and residential areas are discharged into various water resources, necessitating facile analytical techniques for their detection.[2] While innovative devices for online monitoring, such as dissolved oxygen, temperature, turbidity, pH, and conductivity, have made rapid progress in the past two decades,[3−6] traditional spectroscopy is employed for measuring the four conventional indices of chemical oxygen demand (COD), ammonia (N-NH_4), total nitrogen (TN), and phosphates (P-PO_4). Despite the advantages of spectroscopic methods, including sensitivity and reproducibility, their high cost and complex analysis procedures hinder achieving "online monitoring".[7] Given the challenges posed by the diverse and abundant compounds in surface water monitoring, electronic tongues (ETs) are emerging as a promising tool for facile, sustainable, and environmentally friendly online monitoring of water resources.[8] ET involve the utilization of sensor arrays with stoichiometry processing.

In recent years, a plethora of studies has documented the widespread application of ET in environmental water quality monitoring, encompassing the detection and classification of heavy metals,[9,10] inorganic pollutants,[11,12] organic pollutants,[13,14] and microorganism contamination.[15,16] Mimendia et al.[10] applied an 11-electrode potential sensor array for monitoring Cd(II), Cu(II), Pb(II), and Zn(II) in open streams. Belikova et al.[17] conducted continuous online monitoring of ammonium and nitrate in aeration plant treated water using a sensor array of 23 electrodes. Campos et al.[18] explored the use of an 8-metal electrode sensor array in influent and effluent samples from wastewater treatment plants to determine ammonium, sulfates, and phosphates. Wang et al.[19] employed a nanoparticle-modified voltammetry sensor array for evaluating COD in farmland wastewater. Ceto et al.[20] utilized a 4-electrode voltammetry sensor array to monitor the photodegradation of catechol, *m*-cresol, and guaiacol mixtures in wastewater. Legin et al.[21] applied multisensor arrays to assess water environmental safety at two different wastewater treatment plants in St. Petersburg. Regretfully, there have been scarce reports on the online monitoring of COD, TN, N-NH_4, and P-PO_4 in recent years.

Received: January 5, 2024
Revised: May 29, 2024
Accepted: June 7, 2024
Published: June 25, 2024

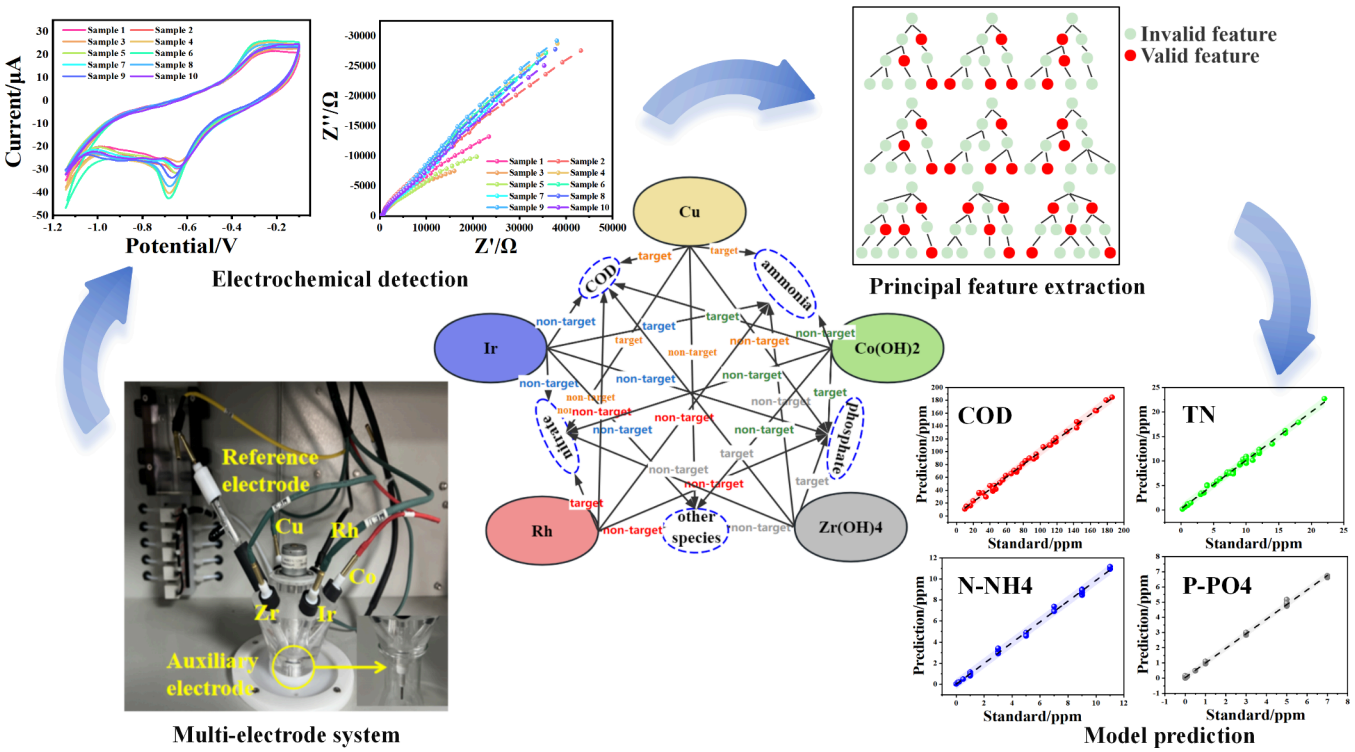

Figure 1. Schematic diagram of the fundamental strategy for simultaneously monitoring COD, TN, N-NH_4, and P-PO_4 in surface water using a 5-electrode multielectrode system.

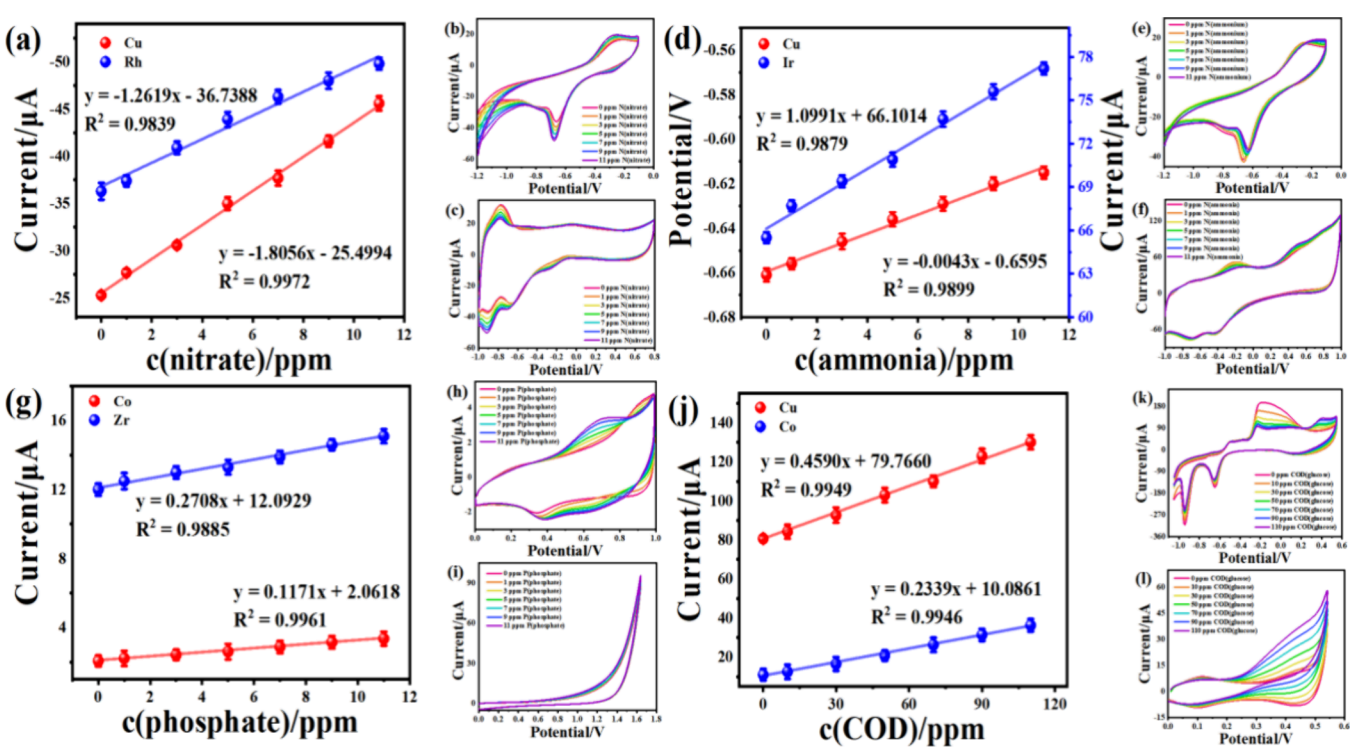

Figure 2. Electrochemical response characteristics of Cu, $Co(OH)_2$, $Zr(OH)_4$, Ir, and Rh electrodes to glucose, nitrate, ammonia, and phosphorus. (a) Response evaluation curves of Cu and Rh electrodes to nitrate nitrogen. (b,c) Corresponding cyclic voltammetry curves. (d) Response evaluation curves of Cu and Ir electrodes to ammonia and (e,f) corresponding cyclic voltammetry curves. (g) Response evaluation curves of $Co(OH)_2$ and $Zr(OH)_4$ electrodes to phosphate and (h,i) corresponding cyclic voltammetry curves. (j) Response evaluation curves of Cu and $Co(OH)_2$ electrodes to glucose and (k,l) corresponding cyclic voltammetry curves.

In summary, the characteristics of the above-mentioned studies are as follows: First, the lack of a targeted (specific) detection mechanism for sensor arrays. While it is reported that electronic tongues are mainly associated with the

https://doi.org/10.1021/acsomega.4c00169
ACS Omega 2024, 9, 29252−29262

nonspecific use of sensors,[22] the reality is that initial research was based on ion-selective electrode arrays. Second, a singular mode of electrochemical measurement. Sensors are categorized into potential sensors and voltammetry sensors based on practical applications,[22,23] leading to limited data dimensions being collected. Third, an emphasis is placed on data processing. The goal is to employ machine learning methods to compensate for sensor interference, drift, or nonlinearity, aiming to achieve classification of different samples or multiple species determination. From a practical perspective, the selection of a sensor array is crucial, directly influencing the detection sensitivity and complexity of the chemical quantitative model. A recent trend to enhance the performance of ETs involves combining sensors with different properties to gather more comprehensive information about the sample.

In this study, a multielectrode system composed of five electrodes (Cu, Ir, Rh, $Co(OH)_2$, and $Zr(OH)_4$) is proposed for configuration of a sensor array to monitor COD, TN, N-NH_4, and P-PO_4 in surface water. The characteristics of our research are highlighted in three aspects: First, the selection of sensor electrodes is based on specific signals for each indicator. Each of the four water quality indicators is selectively detected by at least two electrodes, each employing distinct selectivity mechanisms. Second, a diversity of electrochemical measurement methods is employed. Due to the differing principles of specific response among different electrodes, various electrochemical measurement modes are utilized, including cyclic voltammetry, potential measurement, and impedance spectroscopy. Third, the establishment of the quantitative recognition model relies on extracting important signals. In complex samples without pretreatment or preconcentration steps, sensors are susceptible to interference from electrode material transformation and sample matrix differences, resulting in a multitude of nontargeted (nonspecific) signals in the collected electrochemical data. The application of the Least Absolute Shrinkage and Selection Operator (LASSO) for dimensionality reduction and extraction of essential signals is employed. The obtained data are then evaluated using multivariate calibration methods, such as Multiple Linear Regression (MLR), Partial Least Squares (PLS), and eXtreme Gradient Boosting (XGBoost). Figure 1 outlines the fundamental strategy for simultaneously monitoring COD, TN, N-NH_4, and P-PO_4 in surface water using a 5-electrode multielectrode system. This study presents a novel technique for the development of online water quality monitoring equipment.

2. RESULTS AND DISCUSSION

2.1. Electrode Selection. The selection of electrodes is crucial, directly impacting detection sensitivity and the complexity of the chemical quantitative model.[24−26] Before performing experiments with multielectrode systems, we conducted voltammetry studies to understand the electrochemical behavior of nitrate, ammonium, phosphate, and glucose on various electrodes—typical ions found in surface water. The electrochemical response of a compound is known to be influenced by both the intrinsic chemistry of the electrode and the redox behavior of the substance.[27] Copper (Cu), cobalt (Co), zirconium (Zr), iridium (Ir), and rhodium (Rh) electrodes were chosen for voltammetric measurements, with their response characteristics illustrated in Figure 2. All studies involving these ions were conducted in water at room temperature, utilizing 0.01 M sodium sulfate as the electrolyte. (COD measurements were carried out in 0.01 M sodium sulfate and 0.067 mM sodium hydroxide systems.)

Numerous studies have documented the utilization of metal electrodes to catalyze the reduction of NO_3^- for detecting nitrate nitrogen in water.[28−30] Metals such as Cu and Rh have proven effective in catalyzing the electric reduction of NO_3^-,[31,32] leading to their selection as targeted detection electrodes for nitrate nitrogen. The cyclic voltammetry of the Cu electrode was conducted in 1−11 ppm potassium nitrate solution with a potential range of −1.15 V to −0.1 V. As depicted in Figure 2b, around −1.15 V, the reduction current increases with the rise in NO_3^- concentration, attributed to the reduction of Cu(I) to Cu(0) and the catalytic reduction of NO_3^- to NO_2^-. To assess the targeting characteristics of the Cu electrode for nitrate, a calibration curve was generated using the reduction current at −1.15 V against the nitrate nitrogen concentration (Figure 2a). The curve exhibited a sensitivity of 1.806 μA/ppm, a coefficient of determination (R^2) of 99.72%, and a detection limit of 0.189 ppm. The Rh electrode undergoes cyclic voltammetry scanning in a 1−11 ppm potassium nitrate solution with a potential range of −1 V to +0.8 V. As depicted in Figure 2c, at approximately −0.9 V, the reduction current increases with the elevation of NO_3^- concentration. This is attributed to the adsorption of NO_3^- on the electrode surface during the desorption process of adsorbed H, leading to its reduction into other nitrogen species. To assess the targeting characteristics of the Rh electrode for nitrate, a reduction current of −0.9 V was used to create a calibration curve for the nitrate nitrogen concentration (Figure 2a). The curve exhibited a sensitivity of 1.262 μA/ppm, a coefficient of determination (R^2) of 98.39%, and a detection limit of 0.211 ppm. Although both Cu and Rh electrodes catalyze the reduction of the NO_3^-, the mechanisms differ fundamentally. The Cu electrode's process involves its own reduction alongside the catalytic reduction of NO_3^-, whereas the valence state of the Rh electrode remains unchanged during this process, resulting in distinct electrode refreshment approaches.

Cu and Ir electrodes were determined as targeted electrodes in response to N-NH_4. In our earlier research, we observed that the complexation of ammonia with Cu alters the reduction potential of Cu(II). The cyclic voltammetry of the Cu electrode was conducted in a 1 to 11 ppm ammonium sulfate solution with a potential range of −1.15 V to −0.1 V. As illustrated in Figure 2e, with increasing ammonia concentration, the reduction peak potential of Cu(II) decreases from −0.645 V to −0.571 V. This phenomenon is attributed to the complexation of CuO with NH_3, forming $[Cu(NH_3)_4]^{2+}$,[33,34] which enhances CuO dissolution and simultaneously promotes the NH_4^+ ion hydrolysis to NH_3. Additionally, the pH at the Cu electrode interface undergoes changes, leading to a shift in the Cu(II) reduction potential. The calibration curve relating reduction potential to ammonia concentration is depicted in Figure 2d. The sensitivity of the curve is 4.3 mV/ppm, with a coefficient of determination (R^2) of 98.99% and a detection limit of 0.192 ppm. Ir possesses excellent dehydrogenation capabilities and high oxygen affinity, enabling effective promotion of the oxidation reaction of ammonia.[35,36] The Ir electrode undergoes cyclic voltammetry scanning in a 1 to 11 ppm ammonium sulfate solution with a potential range of −1 V to +1 V. As depicted in Figure 2f, with increasing ammonia concentration, the oxidation peak current around +0.45 V gradually rises due to Ir−OH catalyzing the oxidation of

https://doi.org/10.1021/acsomega.4c00169
ACS Omega 2024, 9, 29252−29262

ammonia. The calibration curve relating the oxidation current to the ammonia concentration is presented in Figure 2d. The sensitivity of the curve is 1.099 μA/ppm, with a coefficient of determination (R^2) of 98.79% and a detection limit of 0.356 ppm. In summary, the response mechanisms of Cu and Ir electrodes to N-NH_4 are distinctly different.

$Co(OH)_2$ and $Zr(OH)_4$ electrodes were selected as targeted electrodes in response to P-PO_4. Cobalt is a resilient metal that exhibits distinctive selectivity for phosphates and is often chosen as a selective electrode for PO_4^{3-} ions. However, all cobalt-based sensors are constrained by interference from dissolved oxygen and chloride ions, impeding their application in surface water environments. In our prior research, we developed a $Co(OH)_2$ electrode with high sensitivity and long-term stability for phosphate electrochemical sensing. The voltammetry behavior of the electrode in a phosphate solution of 1 to 11 ppm is illustrated in Figure 2h. The PO_4^{3-} ion accelerates the oxidation of Co(II) to Co(III), leading to an increase in the oxidation peak current near +0.7 V. Figure 2g demonstrates a well-linear relationship between the oxidation peak current and phosphorus concentration (R^2 = 0.9961), with a detection sensitivity of 0.117 μA/ppm and a detection limit of 0.019 ppm. The substantial affinity, good biocompatibility, and high chemical inertness to acids and bases of ZrO_2 and $Zr(OH)_4$ for phosphate ions render them effective green phosphorus adsorbents.[37,38] The synthesized $Zr(OH)_4$ electrode underwent cyclic voltammetry scanning in a 1 to 11 ppm ammonium sulfate solution with a potential range of 0 V to +1.65 V. In Figure 2i, the oxidation current near +1.3 V increases with the rise in phosphorus concentration. This is due to the acceleration of the oxidation of adsorbed oxygen on the electrode surface caused by the formation of zirconium phosphate, resulting from phosphate adsorption on the $Zr(OH)_4$ electrode surface. The linear relationship between the oxidation current and phosphorus concentration is depicted in Figure 2g. The sensitivity of the curve is 0.271 μA/ppm; the coefficient of determination (R^2) is 98.85%; and the detection limit is 0.026 ppm. The advantage of $Co(OH)_2$ and $Zr(OH)_4$ electrodes lies in the self-cleaning nature of the reduction process measured by voltammetry, eliminating the need for an additional refresh process.

Cu and $Co(OH)_2$ electrodes were chosen as targeted electrodes for the COD response. The Cu electrode exhibits a commendable ability to generate the active substance Cu(III)-O(OH), showcasing superior redox performance for the oxidation of refractory organic compounds.[39] Cyclic voltammetry was conducted in a glucose solution ranging from 10 to 110 ppm, with a potential range of −1.05 V to +0.55 V. In Figure 2k, Cu(III) catalyzes the oxidation of glucose near +0.4 V, leading to a distinct oxidation peak. The oxidation peak current demonstrates a strong linear relationship with the glucose concentration (Figure 2j). The curve's sensitivity is 0.459 μA/ppm; the coefficient of determination (R^2) is 99.49%; and the detection limit is 4.955 ppm. In Figure 2l, Co(II) oxidizes to Co(III) near +0.1 V and further oxidizes to Co(IV) near +0.4 V while catalyzing the oxidation of glucose.[40] Hence, the oxidation peak current near +0.4 V increases with a rising glucose concentration. Figure 2j illustrates the calibration curve of peak current and glucose concentration with a sensitivity of 0.234 μA/ppm, a coefficient of determination (R^2) of 99.46%, and a detection limit of 4.217 ppm. In summary, each water quality index was specifically detected by at least two electrodes with different selectivity mechanisms, and the targeting performance characteristics of the five electrodes were summarized in Table 1.

Table 1. Targeting Performance Characteristics of Five Electrodes

Electrode	Target	Linear working ranges/ppm	R^2	Limit of quantitation/ppm
Cu	Nitrate	1−11	0.984	0.189
	Ammonia	1−11	0.989	0.192
	COD	10−110	0.995	4.955
$Co(OH)_2$	Phosphate	1−11	0.996	0.019
	COD	10−110	0.995	4.217
$Zr(OH)_4$	Phosphate	1−11	0.989	0.026
Ir	Ammonia	1−11	0.988	0.356
Rh	Nitrate	1−11	0.997	0.211

2.2. Collection of Multidimensional Signals. The final current response observed by the electrode consists of two contributions: non-Faraday and Faraday processes.[41] The latter relies on the presence of oxidation and reduction reactions, while the former originates from the contribution of the solution conductivity. Although the targeted current signal of the multielectrode system is based on the Faraday process, there exists a conductivity bias in the sample series. Electrochemical impedance spectroscopy (EIS) reflects the electron transfer rate at the electrode/electrolyte interface and can effectively identify differences in the solution conductivity. The information provided by the Bode plots significantly compensates for the inherent limitations of the Nyquist plots.[42,43] Therefore, a series of synthetic water samples were measured using a multielectrode system, including cyclic voltammetry (CV) and EIS. For CV measurements, each sample comprised 601-dimensional signals. This included 84 current values and 1 reduction peak potential for the copper electrode in the CV range of −1.15 V to −0.1 V. The cobalt hydroxide electrode recorded 80 current values within the CV range of 0 V to +1 V. The zirconium hydroxide electrode yielded 132 current values in the CV range of 0 V to +1.65 V. The iridium electrode produced 160 current values within the CV range of −1 V to +1 V. Lastly, the rhodium electrode generated 144 current values within the CV range of −1 V to +0.8 V. For EIS measurements with 60 frequency points, we obtain 900 dimensions (180 per electrode), covering real and imaginary impedance parts, along with phase angle data. In summary, each sample provides a comprehensive data set with a dimensionality of 1501.

The 160 synthetic water samples were supplemented with other ions commonly found in surface water (Cl^-, CO_3^{2-}, and Mg^{2+}), and their real concentrations of COD, N-NH_4, TN, and P-PO_4 were determined using laboratory methods. Glucose and potassium hydrogen phthalate were employed as standard materials for COD analysis (1 ppm of glucose corresponds to 1.067 ppm of COD, 1 ppm of potassium hydrogen phthalate corresponds to 1.176 ppm of COD). Ammonium sulfate was utilized as the standard material for N-NH_4 analysis, while potassium hydrogen phosphate served as the standard material for P-PO_4 analysis. Ammonium sulfate and potassium nitrate were used as TN standard substances (the total content of nitrogen is the TN value). The types of added standard substances along with their respective concentration ranges are detailed in Table 4. A multielectrode system was employed for

https://doi.org/10.1021/acsomega.4c00169
ACS Omega 2024, 9, 29252−29262

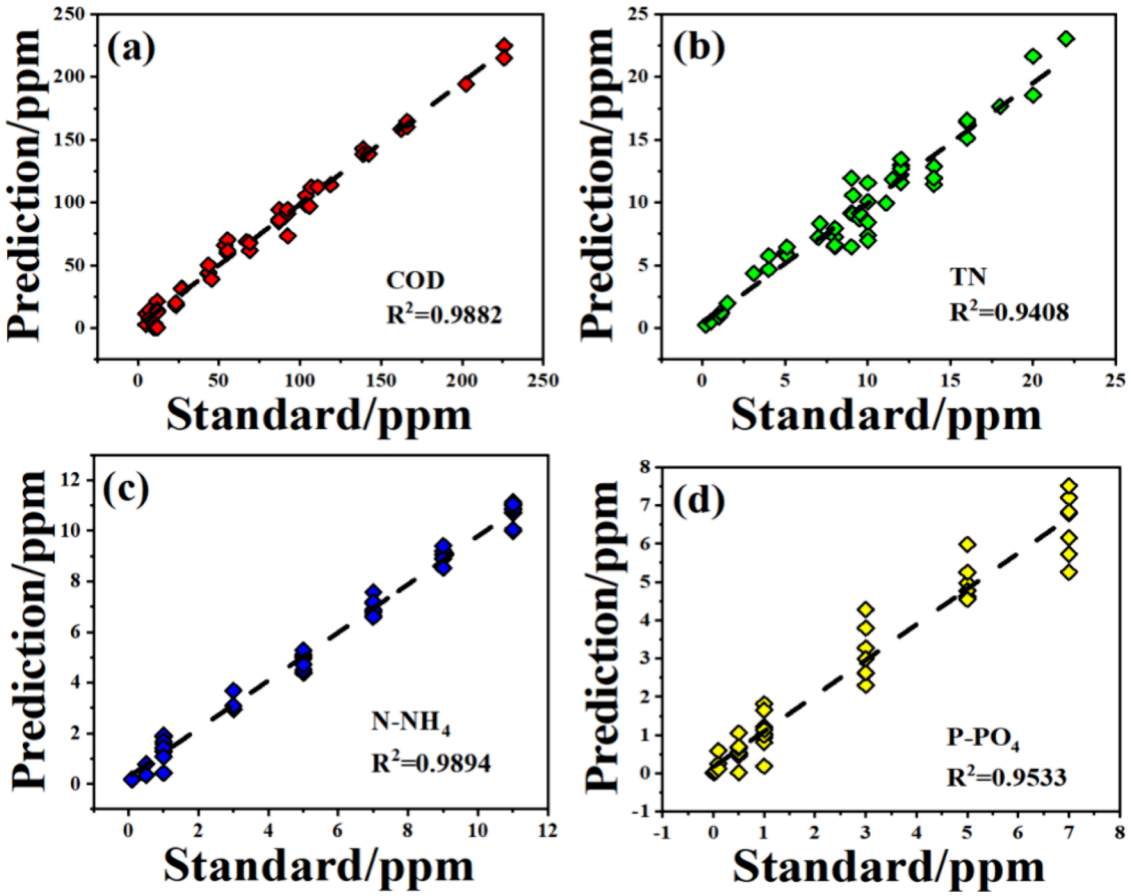

Figure 3. Results of MLR prediction in the 48 validation samples of (a) COD; (b) TN; (c) N-NH_4; and (d) P-PO_4.

sample characterization. Notably, the signal acquisition study spanned several weeks, potentially leading to corrosion processes on the metal electrode during measurements over time. Hence, careful examination of baseline drift was conducted for each electrode. Prior to daily measurements, the multielectrode system underwent refreshing in a 0.01 M sodium sulfate solution (as described in section 4.4) for baseline measurements. Figure S1a−e presents the normalized baseline measurements of five electrodes over 8 days, accompanied by their respective original voltammetry curves, demonstrating that the baseline remained relatively stable after normalization treatment.

The voltammetry response and impedance response of the multielectrode system to different samples are illustrated in Figures S2 and S3, respectively, demonstrating the resolution capability of the 5 electrodes toward diverse samples. Detailed information regarding the 10 selected samples is presented in Table S1. Each sample encompasses a multidimensional signal encompassing CV current value, Cu electrode reduction peak potential, real and imaginary components of the Nyquist diagram, and the phase angle in the Bode diagram. To assess the efficacy of this multielectrode system for synthetic water sample measurements, principal component analysis (PCA) was employed. PCA was conducted on all normalized multidimensional signals from these samples, reducing 1501 signals to 2 principal components. The cumulative reliability of these first two principal components reached 83.33%. The resulting PCA score image is depicted in Figure S1f. Notably, all 160 data points were evenly distributed throughout this image without any discernible boundaries between regions occupied by different colored points, thereby affirming the validity of our collected data.

2.3. Establishment of the Quantitative Identification Model. To address the issue of overfitting in multivariable models, penalty regression estimation methods such as LASSO have gained significant popularity as a feature variable extraction technique.[44] To implement the LASSO regression, an L1 regularization term is incorporated into the objective function. The L1 term represents the absolute value of the regression coefficient multiplied by the sum of regularization parameters, thereby controlling the strength of regularization. Consequently, the regularized LASSO objective function is expressed as follows:

$$J(\beta) = \min\left\{\frac{1}{2n}\sum_{i=1}^{n}(y_i - X_i\beta)^2 + \lambda\sum_{j=1}^{p}|\beta_j|\right\} \quad (1)$$

where β is the regression coefficient; $X_i\beta$ is the predicted value; y is the actual target value; p is the number of features, i.e., the number of variables to be determined; β_j is the jth regression coefficient term; and $\lambda\sum_{j=1}^{p}|\beta_j|$ is to punish the absolute value of the β.

As the regularization parameter λ increases, more coefficients tend to become zero, leading to the exclusion of unimportant features from the model. This reduces the complexity of the model and mitigates the impact of noise.

For the multidimensional signals of 160 synthetic water samples, feature selection and dimension reduction were achieved by adjusting the regularization parameter λ using

https://doi.org/10.1021/acsomega.4c00169
ACS Omega 2024, 9, 29252−29262

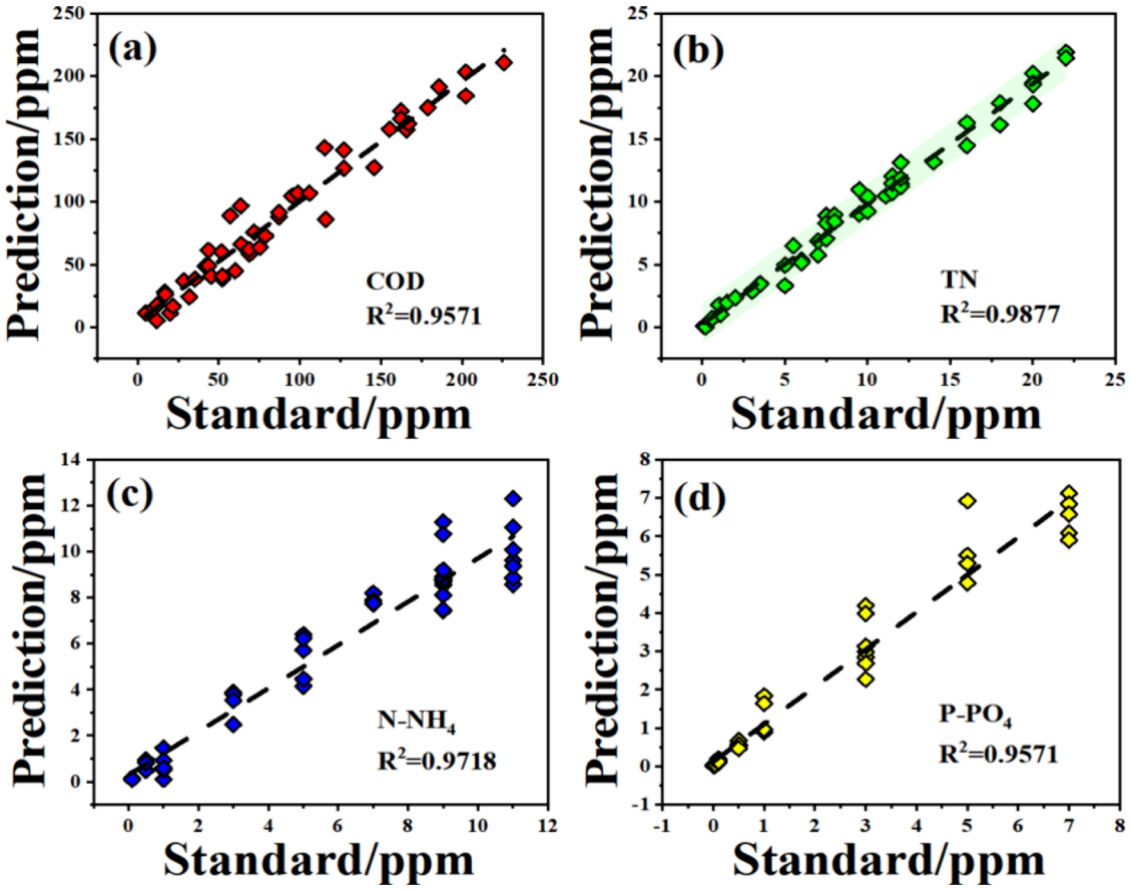

Figure 4. Results of PLS prediction in the 48 validation samples of (a) COD; (b) TN; (c) N-NH_4; and (d) P-PO_4.

the LASSO algorithm. Taking COD as an example, Figure S4a depicts the relationship between λ and the regression coefficient of characteristic variables during the LASSO variable screening process. As λ increases, the coefficient gradually converged toward zero, indicating the elimination of certain variables. Employing cross-validation for parameter selection, Figure S4b illustrates the association between values and errors in the variable selection procedure. The two dashed lines corresponded to λ_{min} = 0.3487 (λ value with the lowest mean error) and λ_{1se} = 0.5059 (the maximum λ value within one standard deviation of the mean error). Ultimately, λ_{min} was determined as the optimal λ value, resulting in the extraction of 77 features comprising the variable set for the COD prediction model.

Specifically, 77, 90, 88, and 79 important features were extracted for COD, TN, N-NH_4, and P-PO_4 to establish a quantitative identification model. To confirm the effectiveness of these signals, signal classification was performed, and an analysis was conducted in conjunction with the targeted signals outlined in Section 2.1. The electrode classification of the signals was presented in Table S2. Clearly, the contribution of the five electrodes to the COD, TN, N-NH_4, and P-PO_4 is fairly uniform, indicating accurate electrode selection. Specifically, Cu, $Zr(OH)_4$, and Ir electrodes exhibit prominent contributions to COD and Cu, Rh electrodes to TN and Cu, Ir electrodes to N-NH_4 and $Co(OH)_2$, and $Zr(OH)_4$ electrodes to P-PO_4. This alignment with the targeted electrodes for different indices in Table 1 showed the correctness of the electrode selection. Furthermore, among the 77 characteristic signals of COD, 32 originate from EIS and 45 from CV. For TN, out of the 90 characteristic signals, 42 are derived from EIS and 48 from CV. In the case of N-NH_4, 44 out of the 88 characteristic signals are from EIS, and 44 from CV. Regarding P-PO_4, 41 out of the 79 characteristic signals are from EIS and 38 from CV. The signals collected through different electrochemical measurement modes exhibit uniformity, emphasizing the necessity of multidimensional signal acquisition. Predominantly, the CV signals for COD are mainly contributed by current values at the highest oxidation potential across the five electrodes, aligning with the oxidation of organic matter and adhering to COD's response principle. TN's CV signal encompasses reduction currents of the Cu electrode (near −1.1 V) and Rh electrode (near −0.9 V), corresponding to the discussed response mechanism in Section 2.1. The concentration of N-NH_4 impacts the reduction peak potential of the Cu electrode and the oxidation current of the Ir electrode (near +0.45 V), all of which are included in the extracted CV signal. Similarly, the concentration of P-PO_4 affects the oxidation current of Co(II) near +0.7 V and the oxygen adsorption on the surface of $Zr(OH)_4$ near +0.3 V, and both signals are also present in the extracted CV signal. In summary, these extracted important features encompass both targeted feature signals and some ambiguous nontargeted signals, demonstrating the effectiveness of the method.

MLR, PLS, and XGBoost analyses were employed to assess the correlation between the predicted values and actual concentrations of COD, TN, N-NH_4, and P-PO_4. A training/verification approach was applied to each parameter, with 160 samples randomly divided into 112 training and 48 validation sets, both of which covered all concentrations.

https://doi.org/10.1021/acsomega.4c00169
ACS Omega 2024, 9, 29252−29262

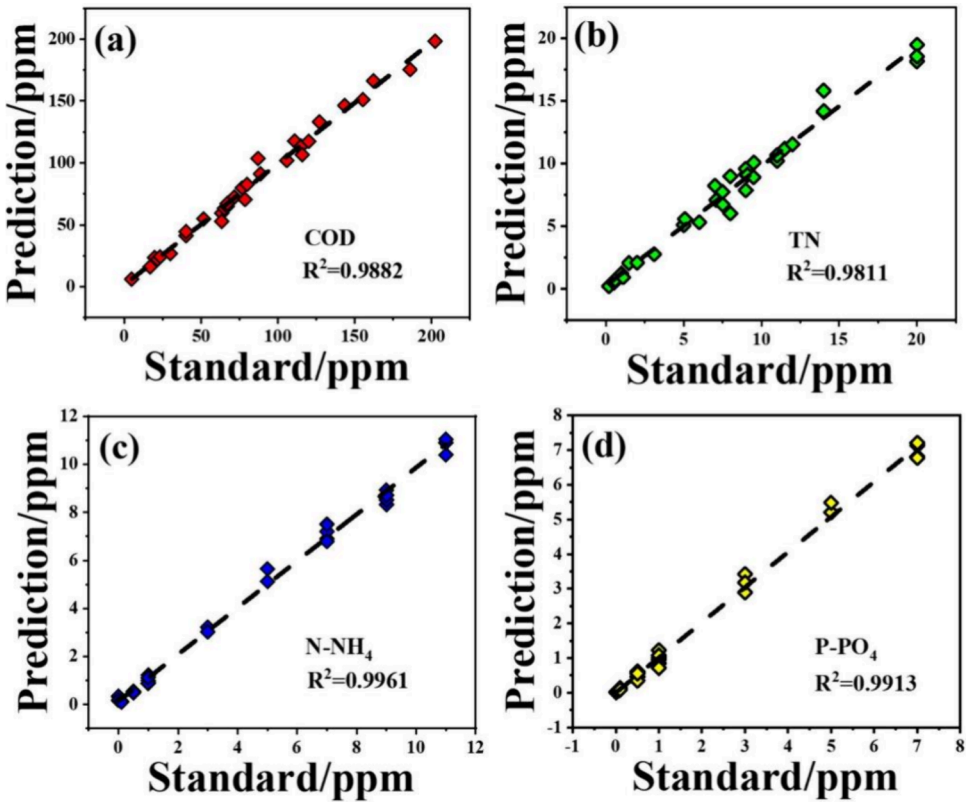

Figure 5. Results of XGBoost prediction in the 48 validation samples of (a) COD; (b) TN; (c) N-NH_4; and (d) P-PO_4.

Table 2. Predictive Performance Parameters of Different Models for Levels of COD, TN, N-NH_4, and P-PO_4

Data analysis	Target	R^2	MAE	RMSE	Concentration range/ppm	APRE
MLR	COD	0.988	5.180	6.550	5−226	23.41%
	TN	0.941	1.013	1.280	0.2−22	13.15%
	N-NH_4	0.989	0.326	0.425	0.1−11	13.81%
	P-PO_4	0.953	0.371	0.545	0.01−7	40.91%
PLS	COD	0.957	10.010	12.930	5−226	21.04%
	TN	0.988	0.606	0.801	0.2−22	11.78%
	N-NH_4	0.972	0.521	0.693	0.1−11	17.58%
	P-PO_4	0.957	0.280	0.518	0.01−7	32.53%
XGBoost	COD	0.988	4.078	5.443	5−226	6.20%
	TN	0.981	0.560	0.778	0.2−22	9.48%
	N-NH_4	0.996	0.198	0.288	0.1−11	7.62%
	P-PO_4	0.991	0.127	0.177	0.01−7	12.54%

Cross-validation was employed to search for the optimal hyperparameters for the three algorithms.[45] The training set facilitated model coefficient derivation, while the validation set assessed the model prediction capability. Figures 3, 4, and 5 depict standard-prediction graphs for each method. Additionally, Table 2 presents predictive performance parameters (R^2, MAE, RMSE, and APRE) for different models applied to a water quality parameter validation set of synthetic samples. Furthermore, Table S3 displays the training set RMSE for the three algorithms.

Multiple Linear Regression (MLR) and Partial Least Squares Regression (PLS) stand out as prevalent methods for modeling quantitative structure−property relationships.[46,47] As depicted in Figure 3, the RMSE values predicted by the MLR model for COD, TN, N-NH_4, and P-PO_4 were 6.550, 1.280, 0.425, and 0.545, respectively. The relationship between the standard and predicted concentrations of TN and P-PO_4 deviated significantly from linearity, with P-PO_4's APRE even exceeding 40%. PLS, as a generalization of regression, is adept at handling data with noise or a large number of X variables, providing a more robust solution compared to MLR. In Figure 4, in contrast to MLR, the R^2 of TN significantly increased from 0.941 to 0.988, and the RMSE decreased by 37.38%. However, the predictive performance of the other three water quality parameters decreased, particularly for COD and N-NH_4 (RMSE increased by 97.40% and 63.06%, respectively), suggesting the need for further optimization of the model.

The XGBoost algorithm stands out as an advanced implementation of gradient-boosted machine learning, known for its efficiency, flexibility, and portability, making it a powerful tool across various forecasting tasks.[48] It is considered one of the top algorithms for supervised regression learning. Currently, XGBoost has found applications in diverse fields such as disaster event prediction, disease prognosis, and runoff

https://doi.org/10.1021/acsomega.4c00169
ACS Omega 2024, 9, 29252−29262

Table 3. Precisions of the Proposed Multielectrode System

	COD	TN	N-NH_4	P-PO_4
Measurement range	5−226 ppm	0.2−22 ppm	0.1−11 ppm	0.01−7 ppm
Limit of quantitation	5 ppm	0.2 ppm	0.1 ppm	0.01 ppm
Precision	±10%/±5 ppm	±10%/±0.2 ppm	±5%/±0.1 ppm	±5%/±0.01 ppm
Reproducibility	±5%	±5%	±3%	±3%
Measuring time	<20 min			

forecasting. 5-Fold cross-validation was employed to ensure the stability of the model's predictive ability, avoiding the overfitting of the XGBoost model. This method uses the folds of data for model construction, while the other fold is used for model validation. Model selection based on the average predicted value can reduce the occasionality caused by overfitting. As illustrated in Figure 5, the predictive model for the four water quality parameters established by the XGBoost algorithm exhibits a significant improvement compared to MLR and PLS. Compared with the MLR algorithm, the predicted RMSE of COD, TN, N-NH_4, and P-PO_4 decreased by 16.9%, 39.22%, 32.24%, and 67.52%, respectively. The R^2 values and APRE values for the prediction models all surpass 0.98 and are below 15%. The predicted ranges for the four water quality parameters are as follows: COD, 5−226 ppm; TN, 0.2−22 ppm; N-NH_4, 0.1−11 ppm; P-PO_4, 0.01−7 ppm. From the above results, the most notable finding is the potential use of a multielectrode system for monitoring COD, TN, N-NH_4, and P-PO_4 concentrations without the need for intricate and time-consuming analytical procedures. From an electrochemical research standpoint, the strong correlation between data from multielectrode systems and the concentrations of COD, TN, N-NH_4, and P-PO_4 is attributed to variations in the electrochemical reactions of electrode groups in the presence of these species.

Furthermore, the electrochemical targeting signal for COD remains identifiable in an alkaline environment and is reliably predicted, even within a neutral electrolyte. The substantial correlation observed between COD and multisensor data is likely attributed to the non-Faraday effect resulting from the partial oxidation of organic products or the adsorption of organic matter on the electrode surface during voltammetric oxidation of metal electrodes. Consequently, the absence of a well-defined redox process does not necessarily impede the utilization of multielectrode systems. Effects such as the non-Faraday effect due to chemisorption on the electrode or the current generated by the reduction or oxidation of water, influenced by the presence of chemical substances, may contribute to the analysis of multidimensional signals. Hence, the acquisition of multidimensional signals proves to be indispensable.

Remarkably, the predictive accuracy for other ions in the synthetic water sample exceeds 0.99, even though their specific electrochemical characteristics have not been deliberately studied. The facile coupling of multielectrode systems to continuously monitor certain parameters, such as Cl^-, CO_3^{2-}, and Mg^{2+}, suggests the potential for their semiquantitative determination in specific water quality scenarios in future implementations.

2.40. Multielectrode System Applied in the Monitoring of Surface Water. In order to assess the performance of the developed multielectrode system, monitoring for COD, TN, N-NH_4, and P-PO_4 concentrations in natural surface water was implemented. Five river water samples and five lake water samples were collected in this study. After a simple filtration operation, the multielectrode system measured multidimensional electrochemical signals. The laboratory methods for the four water quality parameters were as follows: COD determined by the dichromate method;[49] TN determined by ultraviolet spectrophotometry with potassium persulfate digestion;[50] N-NH_4 determined by salicylic acid spectrophotometry;[51] and P-PO_4 determined by ammonium molybdate spectrophotometry.[52] The concentrations of COD, TN, N-NH_4, and P-PO_4 were predicted using the previously established XGBoost model.

Table S4 presents the relative errors between the model predictions and the laboratory methods. The relative error of the multielectrode system in measuring the concentrations of the 4 water quality parameters is approximately 15%. Due to the limited sample size (n = 10) and the absence of a normal distribution, nonparametric tests (Wilcoxon Signed Rank Test) were employed to assess differences between the multielectrode system and the laboratory method. The results of this research hypothesis testing are presented in Table S5, and the P values of 4 water quality parameters were all >0.05. Additionally, the calculated RMSE statistics were as follows: COD = 0.1962, TN = 0.6222, N-NH_4 = 0.2304, and P-PO_4 = 0.0228. Evaluation indicates that there was no significant difference in the measured values between the two methods. In conclusion, the developed multielectrode system demonstrates the potential to replace laboratory methods in monitoring water quality parameters, and the precisions of the proposed multielectrode system are provided in Table 3.

In this study, electrode measurements in the multielectrode system were conducted nonsynchronously, taking approximately 20 min to test a water sample. However, in subsequent implementation applications, modifications to the circuit design enable the synchronized measurement of electrodes, significantly reducing the measurement time to 5 min. The analysis time of the multielectrode system is thereby reduced from hours to minutes, facilitating continuous on-site online monitoring.

3. CONCLUSION

In this study, a novel multielectrode system was developed for the simultaneous determination of COD, TN, N-NH_4, and P-PO_4 using multielement calibration. The results indicate that the system was effectively employed for the quantitative determination of COD, TN, N-NH_4, and P-PO_4 in both river water and lake water. The multielectrode system comprises a set of five metal electrodes (Cu, Ir, Rh, Co$(OH)_2$, and Zr$(OH)_4$). Additionally, the electrodes are self-cleanable and reusable. Each water quality index was specifically detected by at least two electrodes with distinct selectivity mechanisms. Voltammetry characteristics of nitrate, ammonium salt, phosphate, and glucose at different electrodes were reliable.

The multielectrode system effectively provided multidimensional electrochemical signals from synthetic water samples.

https://doi.org/10.1021/acsomega.4c00169
ACS Omega 2024, 9, 29252−29262

The extraction of important characteristic signals was achieved through a combination of normalization and LASSO. The XGBoost algorithm's training set model was applied across various samples (synthetic and real water samples) without requiring complex preprocessing operations. The analysis time of the multielectrode system has been reduced from hours to minutes compared with traditional analysis, facilitating continuous on-site monitoring. Meanwhile, the multidimensional data model successfully predicted almost correct results in the presence of potentially interfering ions (Cl^-, CO_3^{2-}, and Mg^{2+}). This suggests potential applications of multielectrode systems in future implementations for semiquantitative determination of water quality parameters in specific scenarios.

4. EXPERIMENTAL SECTION

4.1. Reagents. Cobalt sulfate heptahydrate was purchased from Aladdin Biochemical Technology (Shanghai, China).

Table 4. Concentration Range of Different Substances in a Synthetic Water Sample

	Target	Concentration range/ppm
Substance	Glucose	5−120
	Potassium nitrate	0.1−11
	Ammonium sulfate	0.1−11
	Potassium hydrogen phosphate	0.01−7
	Sodium chloride	5−60
	Sodium carbonate	3−30
	Potassium hydrogen phthalate	6−90
	Magnesium sulfate	5−60
Index	COD	5−226
	TN	0.1−22
	$N\text{-}NH_4$	0.1−11
	$P\text{-}PO_4$	0.01−7

Sodium phosphate dibasic dodecahydrate, sodium sulfate, sodium hydroxide, and anhydrous ethanol were supplied by Titan Scientific Co., Ltd. (Shanghai, China). Zirconium nitrate pentahydrate, magnesium sulfate heptahydrate, sodium chloride, sodium carbonate, glucose monohydrate, potassium nitrate, ammonium sulfate, and potassium hydrogen phthalate were purchased from Sinopharm Chemical Reagent Co., Ltd. (Shanghai, China). These reagents are commercially procured and utilized without any additional purification treatment throughout the experiment. All of the stock solutions were prepared with deionized water.

4.2. Cyclic Voltammetry. Electrochemical experiments were performed using a CorrTest electrochemical workstation (Wuhan, China). The electrochemical characterization was carried out using different concentrations of glucose, phosphate, ammonium salt, and nitrate, and 0.01 M sodium sulfate was used as the electrolyte. All measurements were performed under ambient temperature conditions (25 ± 1 °C). A Hg/Hg_2SO_4 electrode was used as a reference electrode, and a platinum wire electrode was utilized as the auxiliary electrode during the measurements. The cyclic voltammetry experiments were conducted at a scan rate of 50 mV s^{-1}.

4.3. Preparation of a Multielectrode System. The copper, rhodium, and iridium electrodes were fabricated from commercially available wire (99.9% purity, 1 mm diameter) and securely fixed within a polytetrafluoroethylene tube with a diameter of 6 mm by using an epoxy resin, exposing an effective length of 3 mm.

The preparation of cobalt hydroxide and zirconium hydroxide electrodes consists of two processes: material synthesis and drop coating. Material synthesis: 1.5 g of cobalt sulfate (zirconium nitrate) and 4 g of sodium hydroxide were dispersed into 50 mL of deionized water under magnetic stirring for 20 min. Then, the product was centrifuged at 8500 rpm for 5 min to obtain and then washed with water and ethanol 10 times. Finally, the synthesized cobalt hydroxide and zirconium hydroxide were obtained by drying at 60 °C for 12 h. An amount of 2 mg of synthesized metal hydroxide was evenly distributed in 5 mL of anhydrous ethanol to create a uniform ink through ultrasonication treatment lasting for 30 min. Subsequently, a 5 μL volume of ink was applied onto the cleaned glassy carbon electrode (GCE) measuring 3 mm in diameter and finally dried at room temperature for 20 min.

4.4. Measurement Procedure. The entire measurement system comprises three components: the water inlet and outlet systems, the electrochemical measurement system, and the data transmission system. Seven electrodes, including five working electrodes, one reference electrode, and one auxiliary electrode, are sequentially inserted into the card slot of the glass electrolyzer. The solution's total volume of 5 mL is quantitatively controlled for inflow and outflow by an electronic valve. Before each electrochemical measurement, the electrolytic cell undergoes three cleanings with 0.01 M sodium sulfate to ensure minimal impact from the previous sample on the current one. The measurement steps are configured in the software, encompassing both the electrochemical measurement process and the solution inlet and outlet process. The microcontroller receives data sent by the PC, manages and selects the necessary working electrodes, and performs electrochemical measurements at specified parameters. Simultaneously, the microcontroller's program samples signals corresponding to voltage and current changes at the selected working electrode. The collected data are then transmitted to the PC for processing and storage.

Electrode refresh condition: Electrode refresh was carried out with potentiostatic polarization for 120 s under different potentials in 0.01 M sodium sulfate solution. The copper electrode was at −0.8 V; the iridium electrode was at −1.5 V; and the rhodium electrode was at −1.8 V. The refresh process of the zirconium hydroxide electrode is unnecessary. The cobalt hydroxide electrode needed to be reprepared every day. Each sample was measured 3 times, and the mean was applied in a preprocessing step.

Electrode measurement conditions: Cyclic voltammetry measurements were performed at a scan rate of 50 mV. Copper electrode: −1.15 V ∼ −0.1 V; Cobalt electrode: 0 V ∼ + 1 V; Zirconium electrode: 0 V ∼ + 1.65 V; Iridium electrode: −1 V ∼ + 1 V; Rhodium electrode: −1 V ∼ + 0.8 V. The electrochemical impedance spectroscopy measurement was carried out in the frequency range of 10^6 ∼ 0.1 Hz; the AC amplitude was 10 mV, and 10 times were recorded every decade. Each sample was measured 3 times, and the mean was applied in a preprocessing step.

4.5. Synthetic Samples. The orthogonal table was used to configure 160 synthetic water samples, including COD (glucose and potassium hydrogen phthalate), $N\text{-}NH_4$ (ammonium sulfate), TN (ammonium sulfate and potassium nitrate), $P\text{-}PO_4$ (potassium hydrogen phosphate), Cl^- (sodium chloride), CO_3^{2-} (sodium carbonate), and Mg^{2+} (magnesium

https://doi.org/10.1021/acsomega.4c00169
ACS Omega 2024, 9, 29252−29262

sulfate). 0.01 M sodium sulfate was used as the electrolyte. The concentration ranges of each ion are shown in Table 4.

4.6. Data Preprocessing and Multivariate Analysis. The multivariable principal feature extraction was carried out for all the measured data by LASSO. The 160 synthetic water samples were divided into the training set (112 samples) and the validation set (48 samples) in a 7:3 ratio. MLR, PLS, and XGBoost were used to build a prediction model, and the prediction ability of the test set was compared under these three models. The model evaluation compared the real concentration with the predicted concentration using the correlation coefficient (R^2), root-mean-square error (RMSE), mean relative error (MAE), and average percentage relative error (APRE). All data analysis was carried out in RStudio.

■ ASSOCIATED CONTENT

Supporting Information

The Supporting Information is available free of charge at https://pubs.acs.org/doi/10.1021/acsomega.4c00169.

Images of normalized CV curves of different electrodes in 0.01 M sodium sulfate solution for 8 days, PCA score images of synthetic water sample signals measured on different days, CV results of different electrodes in 10 samples, and Nyquist diagram of different electrodes in 10 samples (PDF)

■ AUTHOR INFORMATION

Corresponding Authors

Defu Liu − *State Key Laboratory of Water Resources and Hydropower Engineering Science, Wuhan University, Wuhan 430072, China*; Email: dfliu@189.cn

Yuqun Xie − *School of Bioengineering and Food Science, Hubei University of Technology, Wuhan 430068, China*; orcid.org/0000-0002-4030-0871; Email: yuqunxie@hbut.edu.cn

Authors

Xinyue Jiang − *State Key Laboratory of Water Resources and Hydropower Engineering Science, Wuhan University, Wuhan 430072, China*

Guodong Jiang − *School of Material and Chemical Engineering, Hubei University of Technology, Wuhan 430068, China*

Complete contact information is available at: https://pubs.acs.org/10.1021/acsomega.4c00169

Author Contributions

Xinyue Jiang: Conceptualization, Methodology, Writing—Original. **Yuqun Xie:** Investigation, Formal Analysis, Writing—Reviewing and Editing. **Guodong Jiang:** Conceptualization, Supervision, Writing—Reviewing and Editing. **Defu Liu:** Funding Acquisition, Project Administration.

Notes

The authors declare no competing financial interest.

■ ACKNOWLEDGMENTS

This work was supported by Yangtze River Water Research Joint Foundation of National Natural Science Foundation of China (grant U2040220).

■ REFERENCES

(1) Cetó, X.; Valle, M. d. Electronic tongue applications for wastewater and soil analysis. *iScience* **2022**, *25* (5), No. 104304.

(2) Gutés, A.; Cespedes, F.; del Valle, M.; Louthander, D.; Krantz-Rülcker, C.; Winquist, F. A flow injection voltammetric electronic tongue applied to paper mill industrial waters. *Sens. Actuators, B* **2006**, *115* (1), 390−395.

(3) Wang, Y. X.; Rinawati, M.; Huang, W. H.; Cheng, Y. S.; Lin, P. H.; Chen, K. J.; Chang, L. Y.; Ho, K. C.; Su, W. N.; Yeh, M. H. Surface-engineered N-doped carbon nanotubes with B-doped graphene quantum dots: Strategies to develop highly-efficient noble metal-free electrocatalyst for online-monitoring dissolved oxygen biosensor. *Carbon* **2022**, *186*, 406−415.

(4) Cheng, W. P.; Hsieh, Y. J.; Yu, R. F.; Huang, Y. W.; Wu, S. Y.; Chen, S. M. Characterizing polyaluminum chloride (PACl) coagulation floc using an on-line continuous turbidity monitoring system. *J. Taiwan Inst. Chem. Eng.* **2010**, *41* (5), 547−552.

(5) Qin, Y.; Alam, A. U.; Pan, S.; Howlader, M. M. R.; Ghosh, R.; Hu, N. X.; Jin, H.; Dong, S.; Chen, C. H.; Deen, M. J. Integrated water quality monitoring system with pH, free chlorine, and temperature sensors. *Sens. Actuators, B* **2018**, *255*, 781−790.

(6) Banna, M. H.; Najjaran, H.; Sadiq, R.; Imran, S. A.; Rodriguez, M. J.; Hoorfar, M. Miniaturized water quality monitoring pH and conductivity sensors. *Sens. Actuators, B* **2014**, *193*, 434−441.

(7) del Valle, M. Sensors as Green Tools. In *Challenges in Green Analytical Chemistry*; Garrigues, S., de la Guardia, M., Eds.; The Royal Society of Chemistry, 2020; p 0.

(8) Vlasov, Y.; Legin, A.; Rudnitskaya, A.; Di Natale, C.; D'Amico, A. Nonspecific sensor arrays ("electronic tongue") for chemical analysis of liquids (IUPAC Technical Report). *Pure Appl. Chem.* **2005**, *77* (11), 1965−1983.

(9) Lu, Y.; Liang, X.; Niyungeko, C.; Zhou, J.; Xu, J.; Tian, G. A review of the identification and detection of heavy metal ions in the environment by voltammetry. *Talanta* **2018**, *178*, 324−338.

(10) Mimendia, A.; Gutiérrez, J. M.; Leija, L.; Hernández, P. R.; Favari, L.; Muñoz, R.; del Valle, M. A review of the use of the potentiometric electronic tongue in the monitoring of environmental systems. *Environ. Model. Software* **2010**, *25* (9), 1023−1030.

(11) Gallardo, J.; Alegret, S.; Munoz, R.; Leija, L.; Hernandez, P. R.; del Valle, M. Use of an Electronic Tongue Based on All-Solid-State Potentiometric Sensors for the Quantitation of Alkaline Ions. *Electroanalysis* **2005**, *17* (4), 348−355.

(12) Nuñez, L.; Cetó, X.; Pividori, M. I.; Zanoni, M. V. B.; del Valle, M. Development and application of an electronic tongue for detection and monitoring of nitrate, nitrite and ammonium levels in waters. *Microchem. J.* **2013**, *110*, 273−279.

(13) Valdés-Ramírez, G.; Gutiérrez, M.; del Valle, M.; Ramírez-Silva, M. T.; Fournier, D.; Marty, J. L. Automated resolution of dichlorvos and methylparaoxon pesticide mixtures employing a Flow Injection system with an inhibition electronic tongue. *Biosens. Bioelectron.* **2009**, *24* (5), 1103−1108.

(14) Roberts, M. G.; Singer, P. C.; Obolensky, A. Comparing TOTAL HAA and TOTAL THM CONCENTRATIONS using ICR data. *J. - Am. Water Works Assoc.* **2002**, *94* (1), 103.

(15) Kirsanov, D.; Legin, E.; Zagrebin, A.; Ignatieva, N.; Rybakin, V.; Legin, A. Mimicking Daphnia magna bioassay performance by an electronic tongue for urban water quality control. *Anal. Chim. Acta* **2014**, *824*, 64−70.

(16) Zadorozhnaya, O.; Kirsanov, D.; Buzhinsky, I.; Tsarev, F.; Abramova, N.; Bratov, A.; Muñoz, F. J.; Ribó, J.; Bori, J.; Riva, M. C.; Legin, A. Water pollution monitoring by an artificial sensory system performing in terms of Vibrio fischeri bacteria. *Sens. Actuators, B* **2015**, *207*, 1069−1075.

(17) Belikova, V.; Panchuk, V.; Legin, E.; Melenteva, A.; Kirsanov, D.; Legin, A. Continuous monitoring of water quality at aeration plant with potentiometric sensor array. *Sens. Actuators, B* **2019**, *282*, 854−860.

(18) Campos, I.; Alcañiz, M.; Aguado, D.; Barat, R.; Ferrer, J.; Gil, L.; Marrakchi, M.; Martínez-Mañez, R.; Soto, J.; Vivancos, J. L. A

voltammetric electronic tongue as tool for water quality monitoring in wastewater treatment plants. *Water Res.* **2012**, *46* (8), 2605−2614.
(19) Wang, Q.; del Valle, M. Determination of Chemical Oxygen Demand (COD) Using Nanoparticle-Modified Voltammetric Sensors and Electronic Tongue Principles. *Chemosensors* **2021**, *9* (3), 46.
(20) Cetó, X.; González-Calabuig, A.; del Valle, M. Use of a Bioelectronic Tongue for the Monitoring of the Photodegradation of Phenolic Compounds. *Electroanalysis* **2015**, *27* (1), 225−233.
(21) Legin, E.; Zadorozhnaya, O.; Khaydukova, M.; Kirsanov, D.; Rybakin, V.; Zagrebin, A.; Ignatyeva, N.; Ashina, J.; Sarkar, S.; Mukherjee, S.; Bhattacharyya, N.; Bandyopadhyay, R.; Legin, A. Rapid Evaluation of Integral Quality and Safety of Surface and Waste Waters by a Multisensor System (Electronic Tongue). *Sensors* **2019**, *19* (9), 2019.
(22) Vlasov, Y.; Legin, A. Non-selective chemical sensors in analytical chemistry: from "electronic nose" to "electronic tongue. *Fresenius J. Anal. Chem.* **1998**, *361* (3), 255−260.
(23) Winquist, F.; Wide, P.; Lundström, I. An electronic tongue based on voltammetry. *Anal. Chim. Acta* **1997**, *357* (1), 21−31.
(24) Wesoły, M.; Przewodowski, W.; Ciosek-Skibińska, P. Electronic noses and electronic tongues for the agricultural purposes. *TrAC, Trends Anal. Chem.* **2023**, *164*, No. 117082.
(25) Gutiérrez-Capitán, M.; Brull-Fontserè, M.; Jiménez-Jorquera, C. Organoleptic Analysis of Drinking Water Using an Electronic Tongue Based on Electrochemical Microsensors. *Sensors* **2019**, *19* (6), 1435.
(26) Mhatre, G. R.; Daurai, B.; Mudhalwadkar, R. P. In Development of electronic tongue for classification of wine with sampling system, *2017 International Conference on Intelligent Computing and Control (I2C2)*, 23−24 June 2017.
(27) Palit, M.; Tudu, B.; Dutta, P. K.; Dutta, A.; Jana, A.; Roy, J. K.; Bhattacharyya, N.; Bandyopadhyay, R.; Chatterjee, A. Classification of Black Tea Taste and Correlation With Tea Taster's Mark Using Voltammetric Electronic Tongue. *IEEE Trans. Instrum. Meas.* **2010**, *59* (8), 2230−2239.
(28) Dima, G. E.; de Vooys, A. C. A.; Koper, M. T. M. Electrocatalytic reduction of nitrate at low concentration on coinage and transition-metal electrodes in acid solutions. *J. Electroanal. Chem.* **2003**, *554*−*555*, 15−23.
(29) Motaghedifard, M. H.; Pourmortazavi, S. M.; Alibolandi, M.; Mirsadeghi, S. Au-modified organic/inorganic MWCNT/Cu/PANI hybrid nanocomposite electrode for electrochemical determination of nitrate ions. *Microchimica Acta* **2021**, *188* (3), 99.
(30) Wang, J.; Zhang, Z.; Wang, S. Facile fabrication of Ag/GO/Ti electrode by one-step electrodeposition for the enhanced cathodic reduction of nitrate pollution. *Journal of Water Process Engineering* **2021**, *40*, No. 101839.
(31) Inam, A. K. M. S.; Costa Angeli, M. A.; Shkodra, B.; Douaki, A.; Avancini, E.; Magagnin, L.; Petti, L.; Lugli, P. Flexible Screen-Printed Electrochemical Sensors Functionalized with Electrodeposited Copper for Nitrate Detection in Water. *ACS Omega* **2021**, *6* (49), 33523−33532.
(32) Casella, I. G.; Contursi, M. Highly dispersed rhodium particles on multi-walled carbon nanotubes for the electrochemical reduction of nitrate and nitrite ions in acid medium. *Electrochim. Acta* **2014**, *138*, 447−453.
(33) Yang, S.; Zang, G.; Peng, Q.; Fan, J.; Liu, Y.; Zhang, G.; Zhao, Y.; Li, H.; Zhang, Y. In-situ growth of 3D rosette-like copper nanoparticles on carbon cloth for enhanced sensing of ammonia based on copper electrodissolution. *Anal. Chim. Acta* **2020**, *1104*, 60−68.
(34) Valentini, F.; Biagiotti, V.; Lete, C.; Palleschi, G.; Wang, J. The electrochemical detection of ammonia in drinking water based on multi-walled carbon nanotube/copper nanoparticle composite paste electrodes. *Sens. Actuators, B* **2007**, *128* (1), 326−333.
(35) Wei, R.-L.; Liu, Y.; Chen, Z.; Jia, W.-S.; Yang, Y.-Y.; Cai, W.-B. Ammonia oxidation on iridium electrode in alkaline media: An in situ ATR-SEIRAS study. *J. Electroanal. Chem.* **2021**, *896*, No. 115254.
(36) Kapałka, A.; Fierro, S.; Frontistis, Z.; Katsaounis, A.; Frey, O.; Koudelka, M.; Comninellis, C.; Udert, K. M. Electrochemical behaviour of ammonia (NH4+/NH3) on electrochemically grown anodic iridium oxide film (AIROF) electrode. *Electrochem. Commun.* **2009**, *11* (8), 1590−1592.
(37) Ju, X.; Hou, J.; Tang, Y.; Sun, Y.; Zheng, S.; Xu, Z. ZrO_2 nanoparticles confined in CMK-3 as highly effective sorbent for phosphate adsorption. *Microporous Mesoporous Mater.* **2016**, *230*, 188−195.
(38) Luo, X.; Wu, X.; Reng, Z.; Min, X.; Xiao, X.; Luo, J. Enhancement of Phosphate Adsorption on Zirconium Hydroxide by Ammonium Modification. *Ind. Eng. Chem. Res.* **2017**, *56* (34), 9419−9428.
(39) Juska, V. B.; Maxwell, G. D.; O'Riordan, A. Microfabrication of a multiplexed device for controlled deposition of miniaturised copper-structures for glucose electro-oxidation in biological and chemical matrices. *Biosens. Bioelectron.: X* **2023**, *13*, No. 100315.
(40) Hu, J.; Lu, H.; Li, M.; Xiao, G.; Li, M.; Xiang, X.; Lu, Z.; Qiao, Y. Cobalt valence modulating in CoOx incorporated carbon nanofiber for enhanced glucose electrooxidation. *Materials Reports: Energy* **2022**, *2* (2), No. 100091.
(41) Barbosa, M. S.; Herrera, J. R.; Santato, C., In situ studies at metal oxide/ionic medium interfaces for electronics and electrochemical energy storage. In *Encyclopedia of Solid-Liquid Interfaces*, 1st ed.; Wandelt, K., Bussetti, G., Eds.; Elsevier: Oxford, 2024; pp 725−742.
(42) Wang, F. M.; Rick, J. Synergy of Nyquist and Bode electrochemical impedance spectroscopy studies to commercial type lithium ion batteries. *Solid State Ionics* **2014**, *268*, 31−34.
(43) Vivier, V.; Orazem, M. E. Impedance Analysis of Electrochemical Systems. *Chem. Rev.* **2022**, *122* (12), 11131−11168.
(44) Shao, Y.; Tang, J.; Liu, J.; Han, L.; Dong, S. Multivariable System Prediction Based on TCN-LSTM Networks with Self-Attention Mechanism and LASSO Variable Selection. *ACS Omega* **2023**, *8* (50), 47798−47811.
(45) Qian, H.; McLamore, E.; Bliznyuk, N. Machine Learning for Improved Detection of Pathogenic E. coli in Hydroponic Irrigation Water Using Impedimetric Aptasensors: A Comparative Study. *ACS Omega* **2023**, *8* (37), 34171−34179.
(46) Riahi, S.; Ganjali, M. R.; Norouzi, P.; Jafari, F. Application of GA-MLR, GA-PLS and the DFT quantum mechanical (QM) calculations for the prediction of the selectivity coefficients of a histamine-selective electrode. *Sens. Actuators B* **2008**, *132* (1), 13−19.
(47) Roy, K.; Pratim Roy, P. Comparative chemometric modeling of cytochrome 3A4 inhibitory activity of structurally diverse compounds using stepwise MLR, FA-MLR, PLS, GFA, G/PLS and ANN techniques. *Eur. J. Med. Chem.* **2009**, *44* (7), 2913−2922.
(48) Wan, A.; Gong, Z.; Chen, T.; Al-Bukhaiti, K. Mass flow characteristics prediction of refrigerants through electronic expansion valve based on XGBoost. *Int. J. Refrig.* **2024**, *158*, 345−352.
(49) Xiao, H.; Yan, W.; Zhao, Z.; Tang, Y.; Li, Y.; Yang, Q.; Luo, S.; Jiang, B. Chlorate induced false reduction in chemical oxygen demand (COD) based on standard dichromate method: Countermeasure and mechanism. *Water Res.* **2022**, *221*, No. 118732.
(50) Lin, K.; Xu, J.; Guo, H.; Huo, Y.; Zhang, Y. Flow injection analysis method for determination of total dissolved nitrogen in natural waters using on-line ultraviolet digestion and vanadium chloride reduction. *Microchem. J.* **2021**, *164*, No. 105993.
(51) Jain, A.; Soni, S.; Verma, K. K. Combined liquid phase microextraction and fiber-optics-based cuvetteless micro-spectrophotometry for sensitive determination of ammonia in water and food samples by the indophenol reaction. *Food Chem.* **2021**, *340*, No. 128156.
(52) Bermejo-Barrera, P.; Moreda-Piñeiro, A.; Bermejo-Barrera, A. Study of ammonium molybdate to minimize the phosphate interference in the selenium determination by electrothermal atomic absorption spectrometry with deuterium background correction. *Spectrochimica Acta Part B: Atomic Spectroscopy* **2002**, *57* (2), 327−337.

https://doi.org/10.1021/acsomega.4c00169
ACS Omega 2024, 9, 29252−29262